



## Iodine solubility in a low-activity waste borosilicate glass at 1000 °C



Brian J. Riley<sup>a,\*</sup>, Michael J. Schweiger<sup>a</sup>, Dong-Sang Kim<sup>a</sup>, Wayne W. Lukens Jr.<sup>b</sup>, Benjamin D. Williams<sup>a</sup>, Cristian Iovin<sup>a</sup>, Carmen P. Rodriguez<sup>a</sup>, Nicole R. Overman<sup>a</sup>, Mark E. Bowden<sup>a</sup>, Derek R. Dixon<sup>a</sup>, Jarrod V. Crum<sup>a</sup>, John S. McCloy<sup>c</sup>, Albert A. Kruger<sup>d</sup>

<sup>a</sup> Pacific Northwest National Laboratory, Richland, WA 99352, United States

<sup>b</sup> Lawrence Berkeley National Laboratory, Berkeley, CA 94720, United States

<sup>c</sup> School of Mechanical and Materials Engineering, Washington State University, Pullman, WA 99164, United States

<sup>d</sup> U.S. Department of Energy, Office of River Protection, Richland, WA 99352, United States

### ARTICLE INFO

#### Article history:

Received 18 February 2014

Accepted 21 April 2014

Available online 30 April 2014

### ABSTRACT

The purpose of this study was to determine the solubility of iodine in a low-activity waste borosilicate glass when heated inside an evacuated and sealed fused quartz ampoule. The iodine was added to glass frit as KI in quantities of 99.4–24,005 ppm iodine (by mass). Each mixture was added to an ampoule, heated at 1000 °C for 2 h, and then air quenched. In samples with  $\geq 11,999$  ppm iodine, low viscosity salt phases were observed on the surface of the melts that solidified into a white coating upon cooling. These salts were identified by X-ray diffraction as mixtures of KI, NaI, and Na<sub>2</sub>SO<sub>4</sub>. Iodine concentrations in glass specimens were analyzed with inductively-coupled plasma mass spectrometry, and the overall iodine solubility was determined to be 10,000 ppm. Several crystalline inclusions of iodine sodalite, Na<sub>8</sub>(AlSiO<sub>4</sub>)<sub>6</sub>I<sub>2</sub>, were observed in the 24,005 ppm specimen.

© 2014 Elsevier B.V. All rights reserved.

### 1. Introduction

The Hanford Site in Washington State has 177 underground storage tanks that contain over 50 million gallons of mixed hazardous high-level waste (HLW) from nuclear weapons production. The U.S. Department of Energy has committed to retrieve, treat, and immobilize this HLW. The Hanford Tank Waste Treatment and Immobilization Plant is being constructed to divide the HLW into high-activity and low-activity waste (LAW) fractions and immobilize them in separate borosilicate glasses. The LAW waste stream is composed primarily of sodium salts with several constituents that cause complications during the vitrification process due to the formation of separate low viscosity alkali-based salt phases on the surface of the glass melt. The Hanford LAW glass produces a version of this salt that is primarily Na<sub>2</sub>SO<sub>4</sub> with small concentrations of halides, CrO<sub>4</sub><sup>2-</sup>, TcO<sub>4</sub><sup>-</sup>, and alkali other than Na [1–4]. In other, non-Hanford LAWs, this salt phase is primarily composed of alkali metal salts of halides and oxyanions (e.g., MoO<sub>4</sub><sup>2-</sup>, SO<sub>4</sub><sup>2-</sup>, CrO<sub>4</sub><sup>2-</sup>, TcO<sub>4</sub><sup>-</sup>) [5–16]. Technetium-99 (<sup>99</sup>Tc), iodine-129 (<sup>129</sup>I), and cesium-137 are of particular concern for salt phase incorporation because their high volatilities can result in low retention in the glass melt during the LAW vitrification process.

However, the major environmental concern with <sup>99</sup>Tc and <sup>129</sup>I is their fast migration in the Hanford site sediments and their long half-lives of  $2.1 \times 10^5$  y for <sup>99</sup>Tc and  $1.6 \times 10^7$  y for <sup>129</sup>I. Iodine-129 is the primary dose contributor during the first 5000 years following disposal according to results of environmental performance assessments conducted to provide assurance that the disposal project for Hanford LAW does not pose undue risk to health and safety [17].

The fraction remaining in the melt relative to the original concentration is defined as the *retention ratio* ( $R_i$ ), which is determined with Eq. (1) where  $g_{i,r}$  is the mass fraction measured after melting and  $g_{i,0}$  is the target mass fraction of the  $i$ -th species [18]. Retention of halides in sodium aluminum borosilicate glass melts decreases consistently with increasing ionic radius where iodine has the lowest retention of the halides, i.e.,  $F > Cl > Br > I$  [18,19]. Recent scaled melter tests with various simulated LAW glass feeds spiked with 1000 ppm iodine (by mass, unless otherwise noted) showed that  $R_i$  for iodine in the LAW glass melt is approximately 20%, on average [20].

$$R_i = g_{i,r}/g_{i,0} \quad (1)$$

The retention of a particular component within a glass melt can be limited by its solubility if the component is present at a concentration comparable to, or above, its solubility. Halide solubility was observed to decrease with increasing ionic radius ( $F > Cl > I$ ) as pre-

\* Corresponding author. Tel.: +1 (509)372 4651; fax: +1 (509)372 5997.

E-mail address: [brian.riley@pnl.gov](mailto:brian.riley@pnl.gov) (B.J. Riley).

sented by Crichton et al. [21] when studying a similar glass composition as that in the current work. They reported that the loss of iodine from volatilization was a major problem even at 900 °C. Dark bubbles, presumably filled with I<sub>2</sub>(g), were observed in glasses containing >2000 ppm iodine. By this criterion, they determined the solubility of iodine to be ~2000 ppm. However, iodine concentrations of 5000–8200 ppm were observed with electron probe microanalysis (EPMA) in the glasses with target concentrations of 10,000 ppm iodine. This inconsistency and the problem of high volatilization with the open crucible melting (although with a lid) technique used in the aforementioned study provide evidence of potential uncertainty in the reported iodine solubility values. Specifically, the main source of uncertainty is whether the iodine solubilities were determined by volatility or by thermodynamic solubility. Additional discussion was provided elsewhere [22] on the correlations between the halides and their respective retentions, solubilities, ionic radii, and bond dissociation energies based on data in the literature [19,21,23].

Recent studies were performed to evaluate the solubilities of <sup>99</sup>Tc both with <sup>99</sup>Tc [24] and with Re [25] as a surrogate for <sup>99</sup>Tc in a LAW glass based on the AN-105 low-sulfur tank waste that has been used in glass formulation studies for assessing Tc retention [26,27]. The solubilities of <sup>99</sup>Tc and Re were determined by melting glass frit with K<sub>2</sub>CO<sub>3</sub> or KReO<sub>4</sub>, respectively, in evacuated and sealed fused quartz ampoules. Sealed ampoules were used to avoid volatile losses during heat treatment at high temperatures. The solubilities were found to be 2000–2800 ppm for <sup>99</sup>Tc [24] and 3000 ppm for Re [25] (~20 mmol/kg in both cases). In the current work, the same approach was used to determine the solubility of iodine in LAW glass. This study was intended to determine if the high volatility observed in melter tests was caused by supersaturation of the silicate melt with iodine. Thus, the order of magnitude of solubility was measured and compared to the order of magnitude of melter feed concentrations.

## 2. Experimental methods

### 2.1. Glass fabrication

The starting material for these experiments was a LAW borosilicate glass that was synthesized with a melt-quench technique. The *baseline* glass, which was the glass without any iodine additions, was made in a large batch from the appropriate amounts of oxides (Al<sub>2</sub>O<sub>3</sub>, Cr<sub>2</sub>O<sub>3</sub>, Fe<sub>2</sub>O<sub>3</sub>, MgO, SiO<sub>2</sub>, TiO<sub>2</sub>, ZnO, ZrO<sub>2</sub>), carbonates (CaCO<sub>3</sub>, K<sub>2</sub>CO<sub>3</sub>, Na<sub>2</sub>CO<sub>3</sub>), H<sub>3</sub>BO<sub>3</sub>, and Na<sub>2</sub>SO<sub>4</sub> (Table 1). The glass batch was homogenized in a vibrating agate mill and melted in a Pt/10%Rh crucible at 1200 °C for 1 h in a Deltech furnace (Deltech, Inc., Denver, CO). The resulting glass was quenched on an Inconel plate and crushed using a tungsten carbide mill within a

vibratory mixer yielding a fine, homogeneous glass powder (<40 μm).

Iodine was added as KI (ChemWest, ~0.5 mm, ACS reagent grade). The target concentration of iodine added to the baseline glass was varied between 99.4 and 24,005 ppm (see Table 1), defined as parts per million of elemental iodine in the glass (by mass). Except for the 99.4 and 1000 ppm samples, KI was ground by hand in an agate mortar and pestle to a fine powder prior to mixing it with the glass frit. The initial tests with 99.4 and 1000 ppm iodine used granular KI, which resulted in a few KI particles that did not fully react with glass during the 2-h heat treatment. The relative ratios of the other components in the glasses where iodine was added remained unchanged, and their concentrations were renormalized after accounting for the added KI. The LAW glass powder and the specified amount of KI were mixed in an agate mill for a total mass of 20 g for each experiment. The batches were prepared this way so the iodine was well-mixed with the glass and captured by the glass powder, thus minimizing kinetic effects in controlling the iodine solubility.

Each batch of glass powder was placed into a flat-bottomed, fused quartz tube (GE214; 20 × 25 × 305 mm; C-Quartz, Ferndale, WA), and a fused quartz end cap was inserted into the tube as shown in Fig. 1. The tube was then connected to a vacuum system and evacuated. When the pressure was ~10<sup>-4</sup> Pa, the tube was sealed with an oxygen-propane torch. This vacuum-sealed tube will hereafter be referred to in this paper as the *ampoule*.

After sealing, three type-K thermocouples (OMEGA, Stamford, CT) were connected to the outside of the ampoule with stainless steel wire for temperature monitoring at the top, middle, and bottom of the melt during the heat treatment. The ampoule was then inserted into a Deltech furnace pre-heated to 750 °C. The temperature of the furnace was increased from 750 °C to 1000 °C at a heating rate of 5 °C min<sup>-1</sup>, followed by a dwell of 2 h at 1000 °C. After dwelling, the furnace temperature was lowered to 900 °C for a few minutes, and the ampoule was removed from the furnace and quenched in air within a stainless steel canister. In a separate experiment, a 23,985 ppm iodine glass was processed the same as previously described with one difference where, instead of air quenching the ampoule, it was plunged into a stainless steel canister full of deionized water (i.e., water-quenched).

### 2.2. Preparation for analysis

Once the ampoule was cooled to room temperature, small pieces were removed and set aside for analysis. The remainder of the sample was vacuum-impregnated with EpoThin™ resin (Buehler, Lake Bluff, IL). Once hardened, a ~5- to 7-mm thick section was removed from the center of the cylindrical ingot with a diamond wire saw (CT400, Diamond Wire Technology, LLC, Colorado Springs, CO). The section was polished with an LP-01 Syntrol

**Table 1**

Glass compositions in mass%. \*The second 24,000 ppm sample (23,985 ppm actual iodine) is the water-quenched sample.

Target I (ppm)	Actual I (ppm)	KI	Al <sub>2</sub> O <sub>3</sub>	B <sub>2</sub> O <sub>3</sub>	CaO	Cr <sub>2</sub> O <sub>3</sub>	Fe <sub>2</sub> O <sub>3</sub>	K <sub>2</sub> O	MgO	Na <sub>2</sub> O	SiO <sub>2</sub>	SO <sub>3</sub>	TiO <sub>2</sub>	ZnO	ZrO <sub>2</sub>	Sum
0	0	0.000	6.100	10.000	2.070	0.020	5.500	0.470	1.480	21.000	45.300	0.160	1.400	3.500	3.000	100.000
100	99.4	0.013	6.099	9.999	2.070	0.020	5.499	0.470	1.480	20.997	45.294	0.160	1.400	3.500	3.000	100.000
500	512	0.067	6.096	9.993	2.069	0.020	5.496	0.470	1.479	20.986	45.270	0.160	1.399	3.498	2.998	100.000
1000	1000	0.131	6.092	9.987	2.067	0.020	5.493	0.469	1.478	20.973	45.241	0.160	1.398	3.495	2.996	100.000
2000	1988	0.260	6.084	9.974	2.065	0.020	5.486	0.469	1.476	20.945	45.182	0.160	1.396	3.491	2.992	100.000
4000	4004	0.524	6.068	9.948	2.059	0.020	5.471	0.468	1.472	20.890	45.063	0.159	1.393	3.482	2.984	100.000
8000	8013	1.048	6.036	9.895	2.048	0.020	5.442	0.465	1.464	20.780	44.825	0.158	1.385	3.463	2.969	100.000
12,000	11,999	1.570	6.004	9.843	2.038	0.020	5.414	0.463	1.457	20.670	44.589	0.157	1.378	3.445	2.953	100.000
16,000	16,018	2.095	5.972	9.790	2.027	0.020	5.385	0.460	1.449	20.560	44.351	0.157	1.371	3.427	2.937	100.000
24,000	24,005	3.140	5.908	9.686	2.005	0.019	5.327	0.455	1.434	20.341	43.878	0.155	1.356	3.390	2.906	100.000
*24,000	23,985	3.138	5.909	9.686	2.005	0.019	5.327	0.455	1.434	20.341	43.879	0.155	1.356	3.390	2.906	100.000

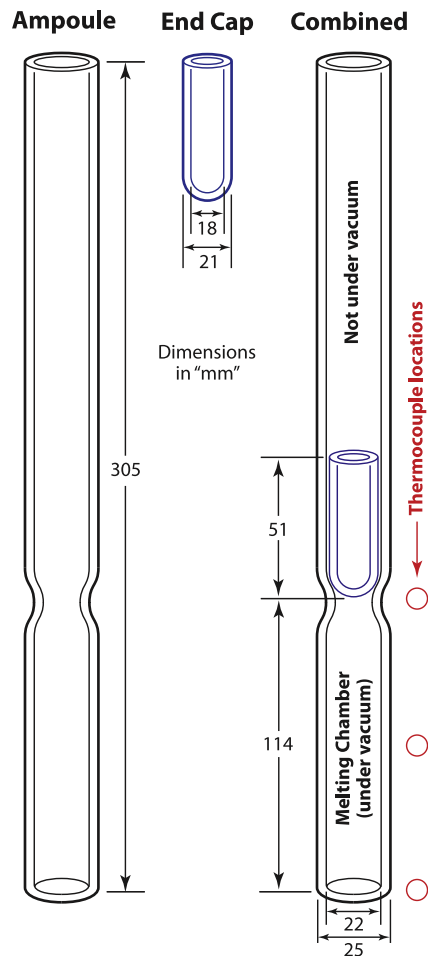


Fig. 1. Schematic of ampoules used for iodine solubility experiments.

vibratory polisher (FMC Technologies, Saltillo, MS) to a 1- $\mu\text{m}$  finish in glycol-based diamond suspensions to help prevent the loss of water-soluble salt inclusions or surface deposits.

### 2.3. Chemical analysis

From each experiment, specimens without visually identifiable inclusions were powdered and analyzed for iodine concentration with inductively-coupled plasma mass spectrometry (ICP-MS) using a Perkin Elmer Elan<sup>®</sup> DRC II (Elemental Scientific, Omaha, NE). Specimens with visually identifiable inclusions were found and analyzed with ICP-MS for comparison to specimens without inclusions using a technique specifically developed at the Pacific Northwest National Laboratory for quantifying iodine [28]. In some cases, specimens with observable inclusions were analyzed as well.

Specimens were ground to a powder in a tungsten carbide mill, 0.01 g of the powder was added to each of two nickel crucibles, and 5 mL of flux solution containing 40% KOH and 4% KNO<sub>3</sub> was then added. Moisture was removed from the flux solution by placing the crucibles in a 150 °C drying oven for 2 h. Crucibles were transferred to a 200 °C furnace that was heated to 550 °C over a 45 min period. The crucibles were then held at 550 °C for 1 h and cooled.

Crucibles were rinsed into 50-mL centrifuge tubes with 5 to 10 mL of deionized water. Each crucible was then rinsed with 5 mL of 1:1 concentrated H<sub>2</sub>SO<sub>4</sub> and 1 M NaHSO<sub>3</sub> (added as Na<sub>2</sub>S<sub>2</sub>O<sub>5</sub>) solution, which was added to the centrifuge tube. Each crucible was rinsed into the centrifuge tube one last time with

deionized water. The contents of the tube were brought to a final volume of 30–35 mL and then analyzed for <sup>127</sup>I with ICP-MS.

### 2.4. X-ray absorption near-edge spectroscopy

X-ray absorption near-edge spectroscopy (XANES) was performed on fragments of selected glasses and powdered iodine standards to identify iodine species. Data were obtained at the Stanford Synchrotron Radiation Lightsource (SSRL) BL 11-2 in transmission (standards) and fluorescence (glass) modes. Data were obtained from 300 eV below the iodine K-edge to 1000 eV above the edge. The data from 75 eV below the edge to 200 eV above the edge were obtained with 0.35-eV spacing; the remaining data points were widely spaced (50 eV) and were used for the pre- and post-edge corrections.

The monochromator was detuned 50% to reduce the harmonic content of the beam. Transmission data were obtained using Ar-filled ion chambers. Fluorescence data were obtained using a 100-element Ge detector and were corrected for detector dead time and self-absorption. Data were reduced from raw data to spectra using SixPack [29], and spectra were normalized using Artemis [30]. Normalized spectra were fit using standard spectra in Fites, a locally written program. Standard spectra were energy-calibrated using NaIO<sub>3</sub> as the energy reference. Spectra of the specimens were allowed to vary in energy during fitting. The spectral resolution was 10 eV based on the width of the NaIO<sub>3</sub> pre-edge peak.

The iodide and iodate standards were prepared by finely grinding the salt with boron nitride and then placing the mixture in an aluminum holder sealed with Kapton<sup>®</sup> tape. All specimens were dried under vacuum and were prepared in an inert atmosphere glovebox and stored in a sealed glass jar until just prior to data collection. The iodine sample was prepared by mixing iodine crystals and boron nitride in a glass vial, heating the vial to 120 °C for 5 min, and then allowing the vial to cool to room temperature. The mixture was heat-sealed inside a thick-walled polyethylene tube (i.e., a disposable pipette). Glass specimens were mounted directly to a sample holder using a tape adhesive.

### 2.5. X-ray diffraction

X-ray diffraction (XRD) analysis was conducted on selected glass and salt specimens with a Bruker<sup>®</sup> D8 Advance (Bruker AXS Inc., Madison, WI) with Cu K $\alpha$  emission ( $\lambda = 1.5406 \text{ \AA}$ ). The detector used was a LynxEye<sup>™</sup> position-sensitive detector with a collection window of 3° 2 $\theta$ . The scan parameters for the glass powders (i.e., 99.4–24,005 ppm iodine) were 5–90° 2 $\theta$  with a step of 0.015° 2 $\theta$  and a 1-s dwell at each step using a 12-mm variable divergent slit. Salts were analyzed in powder mounts from 5° to 70° 2 $\theta$  with a step of 0.015° 2 $\theta$  and a 0.3-s dwell at each step. The salt from the 8013 ppm iodine specimen was analyzed in a sealed 0.6-mm capillary tube from 10° to 80° 2 $\theta$  with a step of 0.015° 2 $\theta$  and a 3-s dwell at each step. Bruker AXS DIFFRAC<sup>plus</sup> EVA and TOPAS software programs were used to identify and quantify the crystalline phases, respectively.

Micro-XRD analysis was conducted on the air-quenched 24,005 ppm iodine glass specimen with a Rigaku D/Max Rapid II micro diffraction system (Rigaku Americas Corporation, The Woodlands, TX). X-rays were generated (MicroMax 007HF operated at 35 kV and 25 mA) from a rotating Cr target ( $\lambda = 2.2910 \text{ \AA}$ ) and focused through a 300- $\mu\text{m}$ -diameter collimator into the specimen. The incident beam direction was fixed at 25° to the specimen surface and the diffracted intensities were recorded on a large two-dimensional image plate. The two-dimensional images were integrated between 25° and 150° 2 $\theta$  to give powder patterns.

## 2.6. Scanning electron microscopy

A JEOL JSM-7001F field emission gun scanning electron microscope (SEM; JEOL USA, Inc. Peabody, MA) was used to analyze specimens. Additionally, an EDAX Si-drift detector was used to conduct energy dispersive spectroscopy (EDS; Apollo XL, AMETEK, Berwyn, PA) for elemental spot analysis and dot mapping.

## 2.7. Electron probe microanalysis and wavelength dispersive spectroscopy

A JEOL JXA-8530F HyperProbe EPMA with a field emission gun and five wavelength dispersive spectrometers (WDSs) was used to conduct area and spot analyses on a polished cross-section of the air-quenched 24,005 ppm iodine glass specimen. The electron beam was set at an accelerating voltage of 15 keV and a probe current of 15 nA. Quantification utilized a ZAF data reduction routine (EPMA Analysis, JEOL) that corrected and quantified characteristic X-ray yields against mineral standards (Geller Microanalytical Laboratory, Inc., Topsfield, MA). The specific standards were SiO<sub>2</sub> for Si, corundum (Al<sub>2</sub>O<sub>3</sub>) for Al, orthoclase (KAlSi<sub>3</sub>O<sub>8</sub>) for K, NaCl for Na, and the 24,005 ppm iodide glass specimen for iodine to identify specific peak locations.

## 3. Results and discussion

### 3.1. General observations

After each ampoule was removed from the furnace, except with the water-quenched 23,985 ppm iodine glass, a dimple formed at the top of the melt upon cooling. This is typical for glass that is air-cooled in a canister. For glasses with as little as 1000 ppm iodine, a faint purple gas was observed inside the ampoule when it was removed from the furnace, and the color faded as the ampoule cooled. This purple haze was observed in all experiments with an increasingly dark purple color at concentrations of >1000 ppm, providing evidence of the presence of I<sub>2</sub>(g). As the ampoule cracked and air penetrated the plenum space, the ampoule walls above the glass turned yellow–brown (1000–4004 ppm iodine glasses) to brown (≥8013 ppm iodine) in color.

For glasses with ≥11,999 ppm iodine, a low viscosity liquid was observed at the top of the melt. This liquid pooled into the dimple and solidified into a white layer on top of the glass upon cooling. This layer appeared very similar to the layer observed in the <sup>99</sup>Tc [24] and Re [25,31] solubility experiments when the amount of added <sup>99</sup>Tc or Re exceeded their solubilities in the glass. The quantity and thickness of this layer increased with iodine loadings ranging from 11,999 → 16,018 → 24,005 ppm, which suggests that the

glass melts with ≥11,999 ppm iodine were oversaturated with alkali iodide at 1000 °C.

### 3.2. Bulk glass analysis

#### 3.2.1. Morphology

In some cases, a full cross-sectional image of each specimen could not be obtained because of severe fracturing that occurred during cooling. A collage of the 99.4-, 1000-, and 11,999-ppm air-quenched specimens and the 23,985 ppm water-quenched specimen is presented in Fig. 2. While cross-sections of the 16,018 and 24,005 ppm air-quenched specimens are not shown, these specimens appeared very similar to the 11,999 ppm specimen. These images reveal that the specimens with increasing iodine concentrations had higher fractions of bubbles throughout the bulk (Fig. 2). The 23,985 ppm water-quenched specimen lacked the characteristic dimple at the top and had a very high fraction of bubbles throughout the bulk, making it difficult to observe any potential inclusions.

#### 3.2.2. Bulk XRD analysis

As seen in Fig. 3, the bulk XRD analysis of glass specimens did not show any diffraction peaks. The diffraction patterns had broad peaks centered around 30–31° 2θ along with other minor peaks at lower and higher angles commonly observed with borosilicate glasses. The diffraction patterns were very similar at different iodine loadings with slight shape variations in location and intensity of the amorphous humps.

#### 3.2.3. XANES analysis

The XANES spectra for NaIO<sub>3</sub>, I<sub>2</sub>, NaI, KI, RbI, CsI, and AgI are shown in Fig. 4 and molecular orbital diagrams for iodide (I<sup>-</sup>), iodine (I<sub>2</sub>), and iodate (IO<sub>3</sub><sup>-</sup>) are shown in Fig. 5. The spectra of NaIO<sub>3</sub>, I<sub>2</sub>, and KI are identical to those previously reported [32–34]. The absorption edge of the NaIO<sub>3</sub> is lowest in energy, followed by I<sub>2</sub> at slightly higher energy. The absorption edges of the iodide salts are almost identical and lie higher in energy. The relationship between the energies of the absorption edges and the formal oxidation state of iodine is reversed from the usual order (i.e., complexes with higher formal oxidation states typically have absorption edges at higher energy). This reversal results from the presence of a large pre-edge peak due to an allowed 1s to 5p transition. This peak is largest for NaIO<sub>3</sub> because the 5p orbitals of iodine are largely vacant in this formally pentavalent complex. The peak is much smaller in I<sub>2</sub> because the 5p orbitals contain five electrons, leaving only a single hole in the σ-antibonding orbital for the 1s electron. The positions of the pre-edge peaks are indicated by arrows in Fig. 4. On the other hand, the 5p shell is filled in the iodide salts, so no pre-edge peak occurs below the absorption edge.

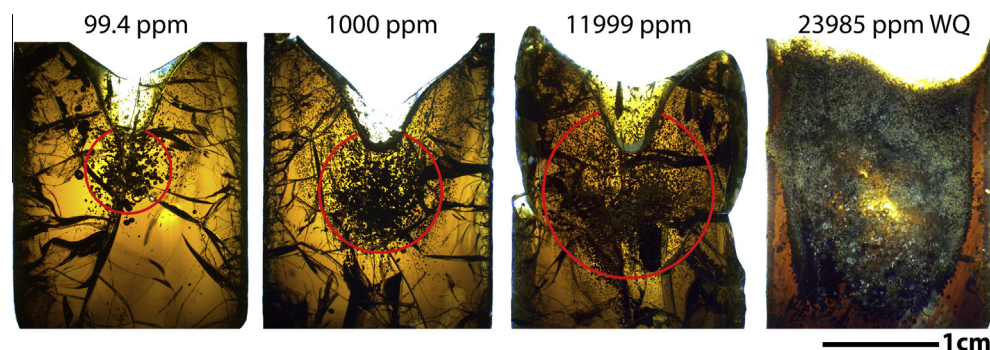


**Fig. 2.** Cross-sectional pictures of 99.4, 1000, 11,999, and 23,985 ppm (water-quenched) glasses. The red outlines represent an approximation of the boundary of bubbles in the 99.4, 1000, and 11,999 ppm iodine glasses. (For interpretation of the references to colour in this figure legend, the reader is referred to the web version of this article.)

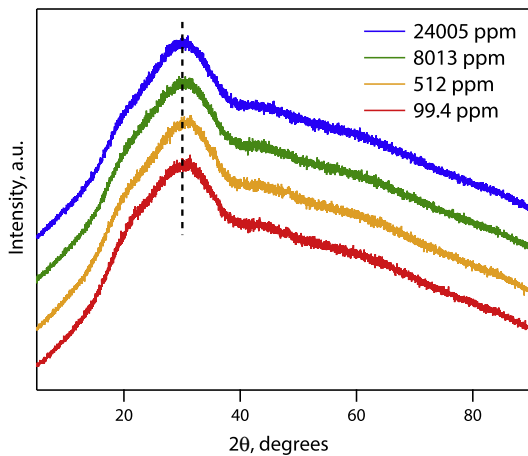


Fig. 3. XRD patterns for powdered glass specimens at 99.4, 512, 8013, and 24,005 ppm iodine loadings. The vertical dotted line is shown as a guide to the eye.

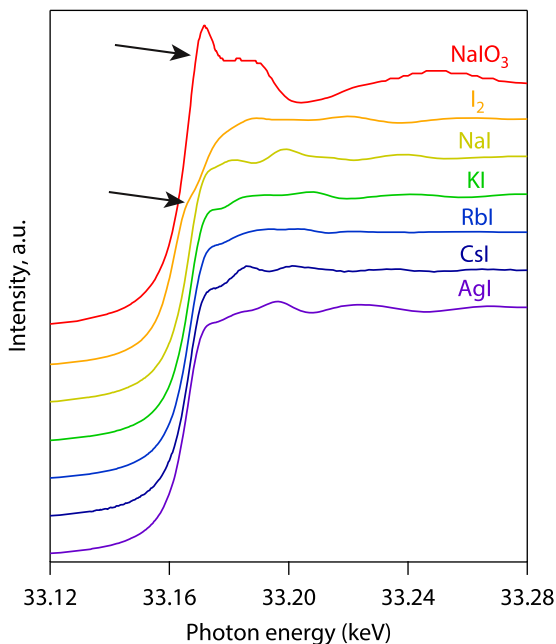


Fig. 4. XANES spectra for iodine standards. The pre-edge features for  $\text{NaIO}_3$  and  $\text{I}_2$  are indicated by arrows.

In addition to the pre-edge peak for  $\text{NaIO}_3$  and  $\text{I}_2$  in Fig. 4, more structures are present in all of the XANES spectra because of scattering of the outgoing photoelectron from the surrounding atoms (extended X-ray absorption fine structure, EXAFS). The EXAFS features are very strong in the case of  $\text{NaIO}_3$ , which possesses three short terminal oxide ligands. On the other hand, the EXAFS spectra are quite weak in  $\text{I}_2$  and the alkali iodides because of the much longer distance from iodine to the surrounding atoms. The frequency of the EXAFS oscillations is inversely proportional to the bond length, so only one broad oscillation is visible for  $\text{NaIO}_3$  (33,188–33,240 eV) with the short I=O bonds, while between three and four oscillations are present in the spectrum of CsI (peaks at 33,186, 33,201, 33,236, and 33,262 eV).

The spectra of the iodine-containing glasses are almost identical. The only real difference is that the 11,999 ppm iodine specimen has a small peak at the edge. Performing the background subtraction was problematic for this specimen (the post-edge

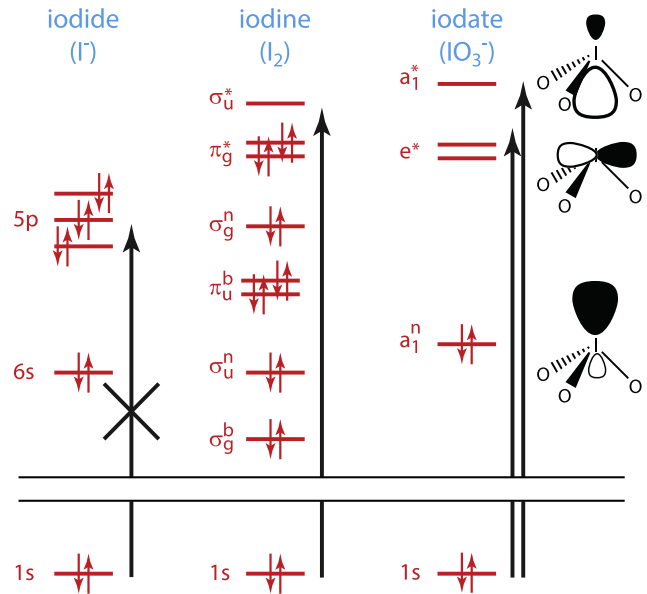


Fig. 5. Molecular orbitals for iodide ( $\text{I}^-$ ), iodine ( $\text{I}_2$ ), and iodate ( $\text{IO}_3^-$ ). No 1s to 5p transition is possible for iodide because all of the 5p orbitals are filled.

region was strongly curved), and this difference may not be meaningful. The spectra of all glasses and their fits are shown in Fig. 6. In all cases, a good, albeit not perfect, fit was obtained and the results are given in Table 2. The glass spectra were initially fit using all seven reference spectra, but only the spectrum of NaI contributed significantly to the fit. Using all of the reference spectra simultaneously resulted in large standard deviations for the contribution of the reference spectra, so the fits were performed using only NaI,  $\text{I}_2$ , and  $\text{NaIO}_3$ .

The significance of the standard spectra in fitting glass spectra is given by the  $p$ -value of that component (the  $p$ -value is the probability that the improvement to the fit results from random error). A  $p$ -value less than 0.05 means that the contribution of that component is greater than twice the standard deviation of the fit, which is the usual criteria for significance in XANES fitting. The NaI contributed significantly ( $p < 0.001$ ) in all cases, and the contribution from  $\text{I}_2$  is significant only when the iodine loading was  $\leq 1988$  ppm iodine. The detection limit is approximately twice the standard deviation or  $\sim 10\%$  of the iodine species. In other words, these XANES results cannot reliably determine the concentration of the species if it comprises less than 10% of the total iodine species. The 1988 ppm glass was run on all three occasions where XANES analysis was performed to assess the reproducibility of the data. As is shown in Table 2, the values for each separate analysis on this glass varied somewhat with 0.79–0.99 for NaI, 0–0.10 for  $\text{I}_2$ , and 0.01–0.11 for  $\text{NaIO}_3$ .

The XANES spectra for iodine in the glass and that from NaI standard did not agree perfectly, which is partially responsible for the relatively large uncertainties in the XANES speciation. Specifically, the EXAFS oscillations of the glass spectra are weaker and lower in frequency relative to NaI. These results suggest that the species present in the glass is iodide surrounded by sodium ions. However, the sodium ions are slightly closer to iodide than they are in the crystal structure of NaI, and there are fewer sodium ions present and/or there is a larger variation in the distances between iodide and the neighboring sodium ions. The fact that the NaI distance is shorter in the glasses is consistent with the hypothesis that there are fewer sodium ions surrounding the iodide in the glass than the six sodium neighbors in the NaI crystal structure. The fact that the XANES spectra of the glass are not perfectly fit by the

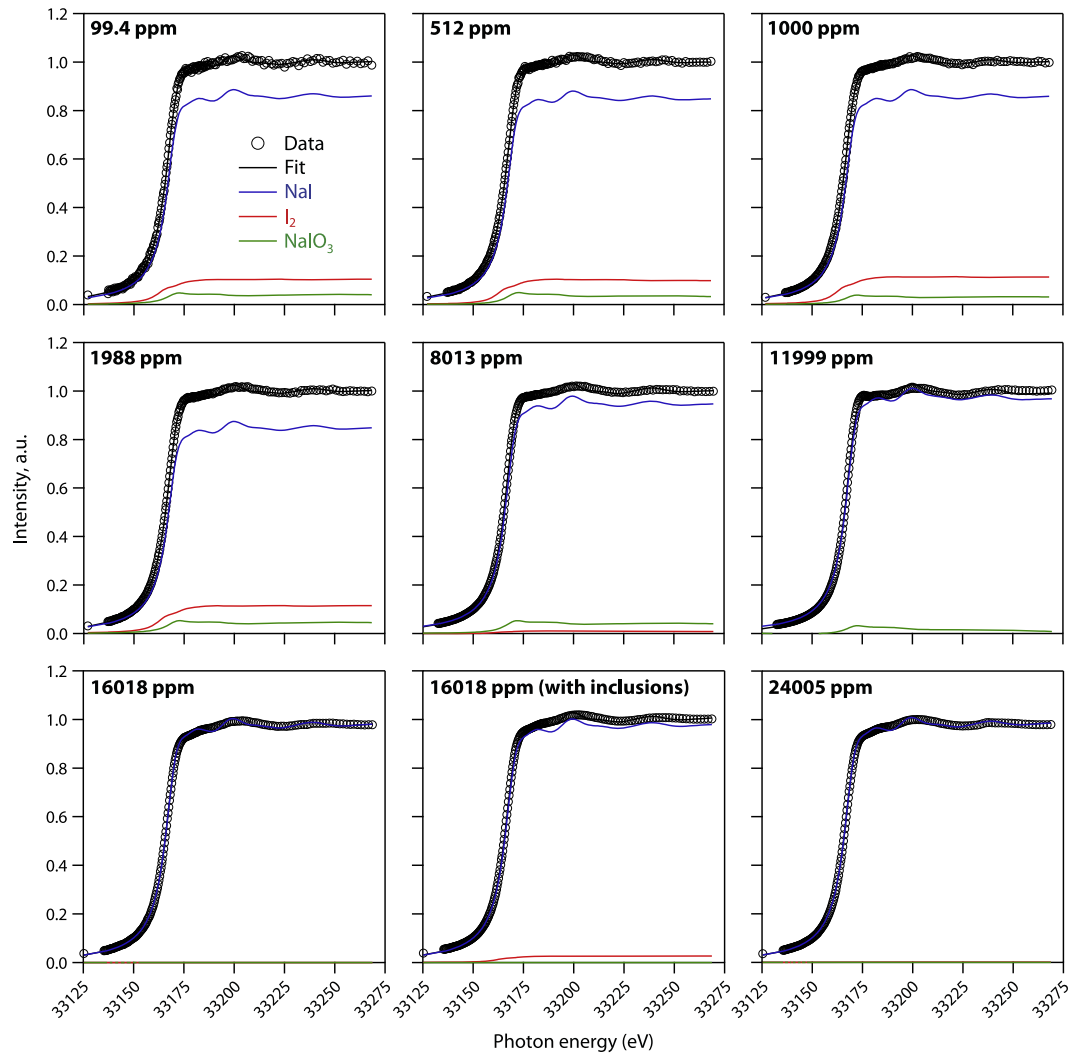


Fig. 6. Iodine K-edge XANES spectra and fits for iodine-containing glass specimens.

Table 2  
XANES results.

Specimen (ppm iodine)	NaI	$p^*$	I <sub>2</sub>	$p$	NaIO <sub>3</sub>	$p$
99.4	0.8(1)	<0.001	0.10(7)	0.12	0.04(5)	0.40
512	0.85(7)	<0.001	0.11(5)	0.03	0.04(3)	0.21
1000	0.87(7)	<0.001	0.11(4)	0.03	0.03(3)	0.36
1988 <sup>†</sup>	0.79(5)	<0.001	0.10(4)	0.014	0.11(3)	0.001
1988	0.87(7)	<0.001	0.10(4)	0.04	0.04(3)	0.25
1988	0.99(7)	<0.001	0.00(5)	1.00	0.01(4)	0.34
8013	0.94(6)	<0.001	0.01(4)	0.77	0.04(3)	0.15
11,999	1.0(1)	<0.001	0.00(8)	1.00	0.03(6)	0.12
16,018	1.00(8)	<0.001	0.00(6)	1.000	0.00(4)	1.000
16,018 <sup>‡</sup>	0.97(8)	<0.001	0.03(5)	0.509	0.00(4)	1.000
24,005	1.00(7)	<0.001	0.00(5)	0.868	0.00(4)	1.000
24,005 (salt)	1.00(5)	<0.001	0.00(4)	0.729	0.00(3)	1.000
1988 (bubbles)	0.94(6)	<0.001	0.01(4)	0.83	0.05(3)	0.07
8013 (bubbles)	0.90(6)	<0.001	0.04(4)	0.29	0.05(3)	0.10
11,999 (bubbles)	0.99(9)	<0.001	0.00(6)	1.00	0.01(4)	0.49

\* Standard deviation of the fit is given in parentheses. The value of  $p$  is the probability that the improvement to the fit from including this spectrum is due to noise. Components with  $p < 0.05$  are significant at the  $2\sigma$  level and those with  $p < 0.01$  are significant at the  $3\sigma$  level.

<sup>†</sup> The 2000-ppm specimen was run on three separate occasions to determine the repeatability of the analysis. This is the specimen where the goodness of fit was higher when I<sub>2</sub> and NaIO<sub>3</sub> were included (see text).

<sup>‡</sup> This specimen contained noticeable salt inclusions.

spectrum of NaI is more consistent with the presence of  $(\text{Na}^+)_{\text{x}}(\text{I}^-)$  clusters in the glass than with crystalline NaI inclusions. The presence of  $(\text{Na}^+)_{\text{x}}(\text{I}^-)$  clusters rather than crystalline NaI inclusions is also supported by the bulk XRD analyses discussed above.

### 3.3. Iodide precipitates

#### 3.3.1. Melt surface salts

The salts observed on top of the melt in  $\geq 11,999$  ppm iodine specimen were removed and analyzed with SEM, XRD, and XANES. The SEM of representative salts for the 16,018 ppm iodine specimen are shown in Fig. 7. The XRD of the salts from the 11,999, 16,018, and 24,005 ppm iodine experiments analyzed in air showed mixtures of NaI·2H<sub>2</sub>O, Na<sub>2</sub>SO<sub>4</sub>, and KI. A typical XRD pattern for one of these salt mixtures is presented in Fig. 8 for the 16,018 ppm iodine specimen. A specimen of the 24,005 ppm iodine salt was analyzed in a sealed capillary tube (not shown) and it was confirmed that the NaI was not initially hydrated. Thus, the NaI became hydrated, forming NaI·2H<sub>2</sub>O upon exposure to the atmosphere during the analysis of the specimens. The XANES analysis confirmed that the primary iodine configuration was in the presence of sodium instead of K (NaI, Table 2). This suggests that KI, the source of added iodine, mixed with sodium from the glass to form NaI, similar to what was observed in the KReO<sub>4</sub>-glass system

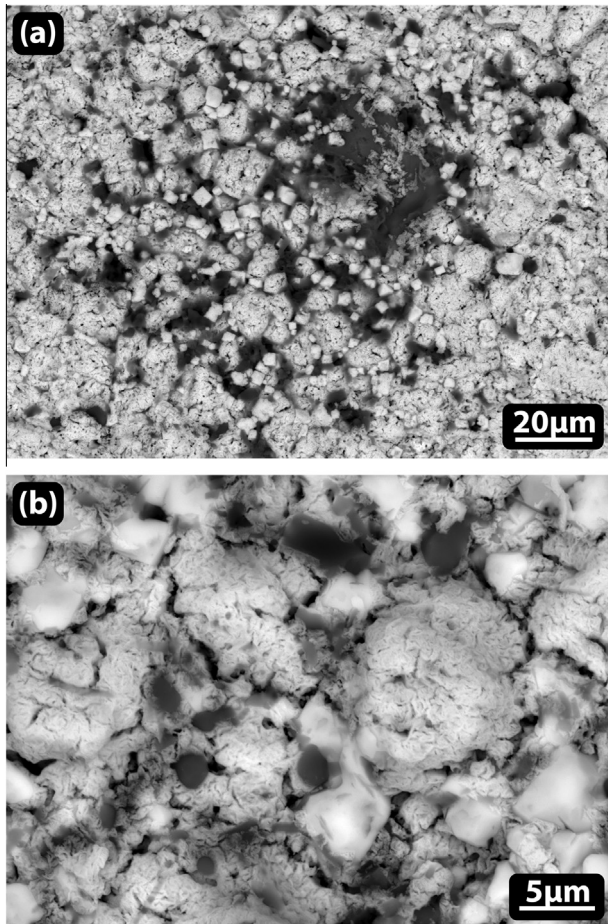


**Fig. 7.** SEM micrographs of mixed salts on top of the 16,018 ppm iodine sample at (a) low and (b) high magnifications. The dark phase is the sulfate and the bright phase is a mixture of the various iodide and iodate salts.

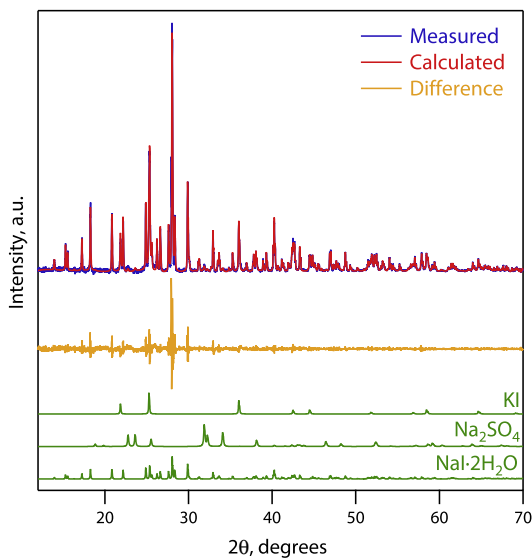


**Fig. 8.** Measured, calculated, difference, and phase XRD patterns for mixed salt on top of 16,018 ppm iodine experiment.

[25,35]. These mixed salt formations are analogous to the formation of Re and  $^{99}\text{Tc}$  salts observed during their respective solubility

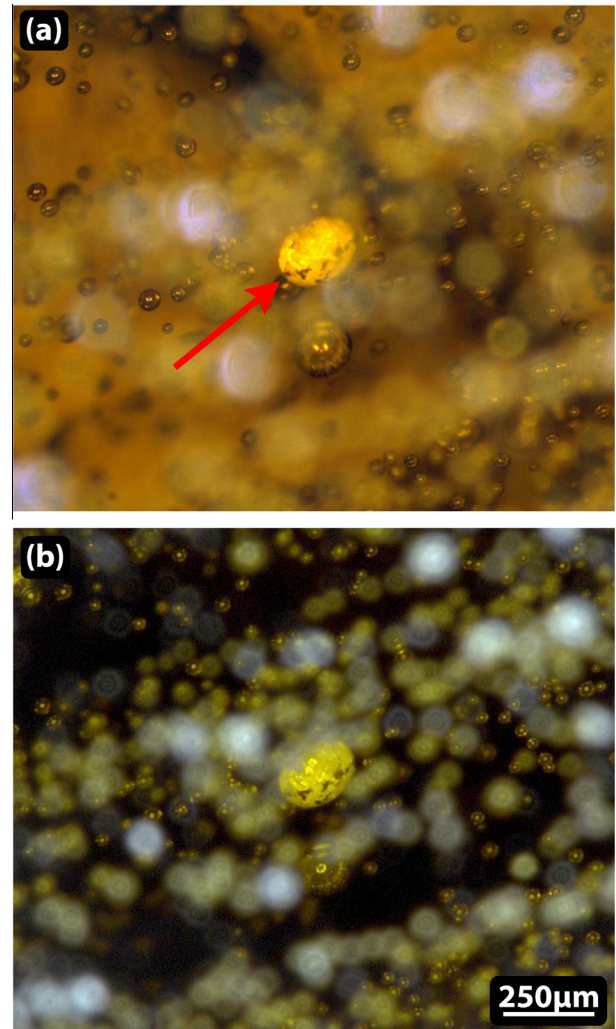


**Fig. 9.** Optical micrographs of a subsurface inclusion in the 11,999 ppm iodine glass in (a) transmitted and reflected light and (b) reflected light.

experiments [24,25]. Similarly, a separate sulfate salt phase is formed during melter processing of waste glass feeds when the amount of sulfate exceeds its solubility in the glass [4,5].

### 3.3.2. Iodine inclusions

**Fig. 9** shows an example of the inclusions found within the glasses with  $\geq 8013$  ppm iodine. In specimens containing 8013 and 11,999 ppm iodine, the inclusions were few, large, and ellipsoidal, ranging in size from 100 to 250  $\mu\text{m}$  along the longest axis. At higher concentrations of 16,018 and 24,005 ppm (i.e., air-quenched) iodine, very small inclusions were observed in addition to the large inclusions. The very small inclusions were too small to analyze individually but the larger inclusions were visible on the polished surface or were only slightly below the surface and could be extracted with tweezers for further analysis.

An SEM micrograph and a WDS area map were collected of a cross-sectioned inclusion and the results are presented in **Fig. 10**. This inclusion also was analyzed with micro-XRD and was determined to be a NaI-based sodalite with a composition of  $\text{Na}_8(\text{AlSiO}_4)_6\text{I}_2$ , space group of  $P43n$ , and a unit cell  $a = 0.9027$  nm [36] with Rietveld refinement using whole-pattern fitting software according to the fundamental parameters approach [37] (**Fig. 11**). The structure of NaI-based sodalites consists of Na–Al–Si–O cages

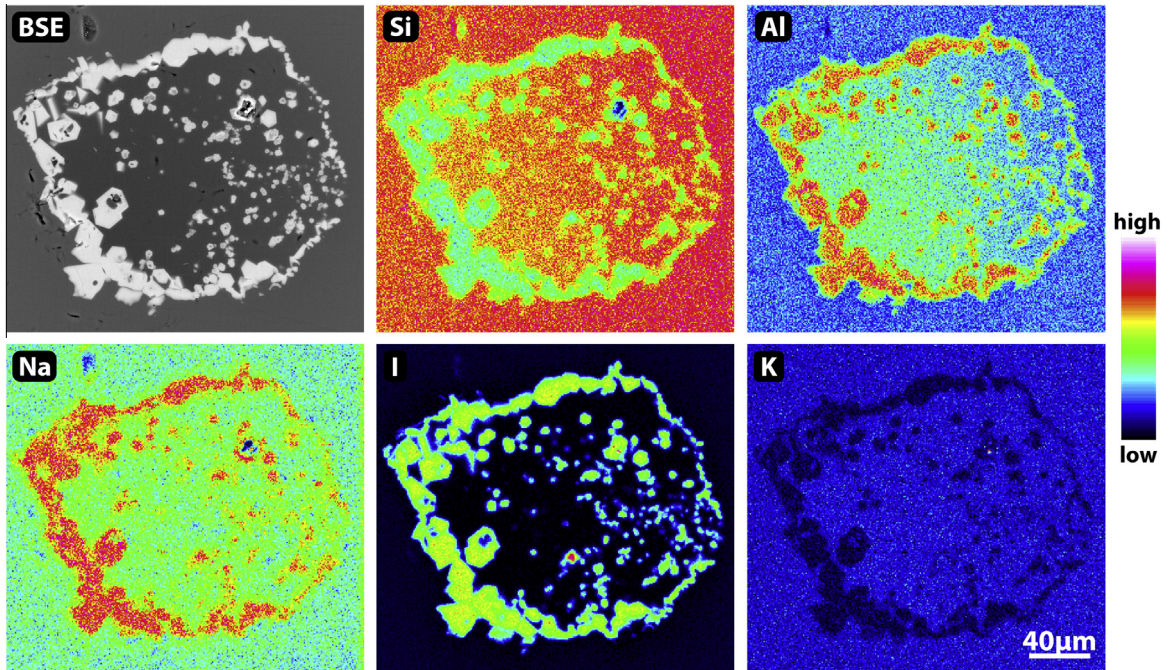


**Fig. 10.** Backscattered electron (BSE) micrograph and EPMA-WDS elemental map showing the distribution of Si, Al, Na, I, and K across the iodide sodalite inclusion in the 24,005 ppm iodine (air-quenched) glass.

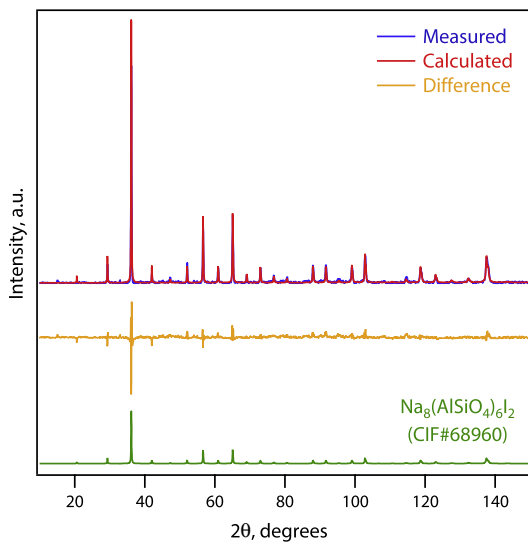


**Fig. 11.** Measured, calculated, and difference spectra for iodide sodalite obtained with micro-XRD.

with iodine atoms in the center and corners of the unit cell shown in Fig. 12.

Spot WDS analysis on inclusions from the 24,005 ppm iodine (air quenched, Fig. 10) is in good agreement (Fig. 13) with the stoichiometric composition of sodalite,  $\text{Na}_8(\text{AlSiO}_4)_6\text{I}_2$ . Other inclusions that were removed with tweezers and observed on polished or fractured cross-sections were also determined to be sodalite with EDS (not shown). In all cases, these inclusions resembled bubbles when examined with optical microscopy, but when cross-sectioned, they were not hollow. Instead, the inclusions were clusters of smaller sodalite crystals,  $\sim 1$  to  $10 \mu\text{m}$  in size, surrounding a pocket of glass with a slightly different composition than the bulk glass. The WDS map in Fig. 10 shows that the sodalite crystals

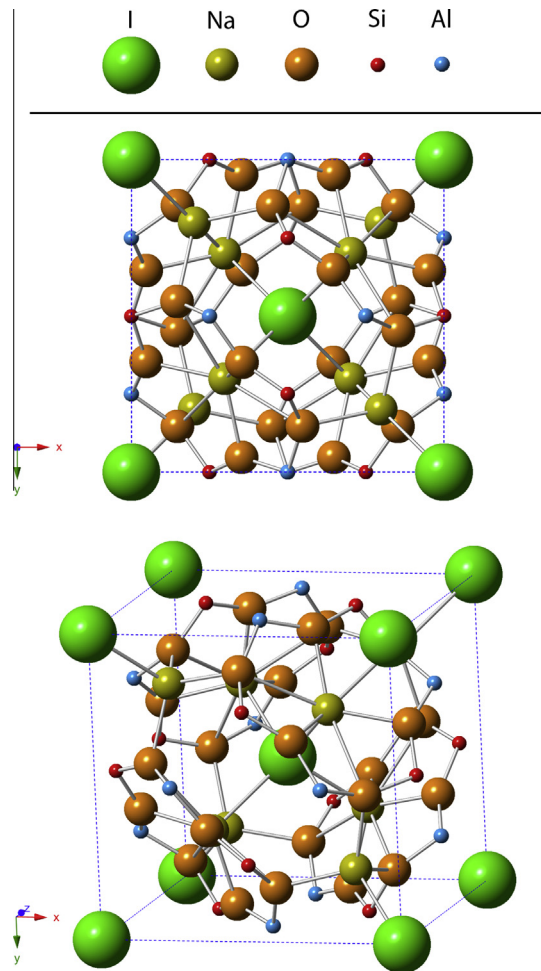


**Fig. 12.** Structure of  $\text{Na}_8(\text{AlSiO}_4)_6\text{I}_2$  according to Weller and Wong [36].

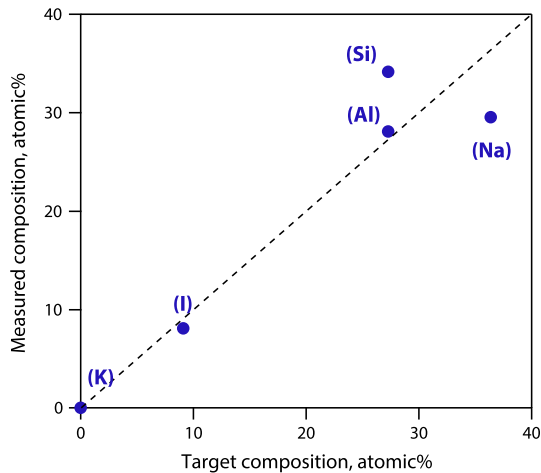


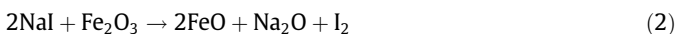
**Fig. 13.** Comparison between stoichiometric (target) element distribution  $[\text{Na}_8(\text{AlSiO}_4)_6\text{I}_2]$  and values measured with WDS spot analysis.

did not contain K, and the Al concentration was higher within the sodalite.

It was not clear whether these sodalite inclusions formed upon soaking at 1000 °C or upon cooling. Thus, the 23,985 ppm iodine water-quenched sample was prepared for this reason; unfortunately, the extremely high number of bubbles present in the water-quenched specimen made the search for inclusions very difficult. Because the sodalite is likely to dissolve in the glass melt at 1000 °C, the sodalite most likely formed during cooling, but additional testing was not performed to support this hypothesis.

### 3.4. Iodine speciation

Various forms of iodine were observed with XANES and XRD. The XANES analysis of the glass specimens showed that the contribution from iodide was significant below 1988 ppm, but iodate was only significant for a single specimen. The presence of  $\text{I}_2$  in contact with the melt is consistent with the characteristic purple gas, which was observed inside the ampoule upon removal from the furnace. For  $\text{I}_2$  or  $\text{IO}_3^-$  to be present in glass, the starting material would require oxidation from  $\text{I}^-$  to  $\text{I}^0$  or  $\text{I}^{5+}$ , respectively. One potential oxidant is  $\text{Fe}^{3+}$ , which comprises ~5% of the glass by mass, as shown in Reactions (2) and (3). In the previous experiments designed for studying  $^{99}\text{Tc}$  solubility with the same glass frit [24], 95.5% of the iron was initially present as  $\text{Fe}^{3+}$ , which decreased to 87% after that frit was run in the baseline experiment at 1000 °C under vacuum in a sealed quartz ampoule. The initial frit and the frit subjected to melting under vacuum both contain a large excess of  $\text{Fe}^{3+}$  relative to  $\text{Fe}^{2+}$ , which could be responsible for the oxidation of iodide observed in this study. Another potential reduction–oxidation (redox) reaction is the disproportionation of  $\text{I}_2$  to  $\text{NaI}$  and  $\text{NaIO}_3$  as shown in Reaction (4). We did not specifically study potential changes in iodine speciation in glasses with different redox conditions.



### 3.5. Solubility

The full data set of measured versus targeted iodine concentration as quantified by ICP-MS is presented in Fig. 14, where the

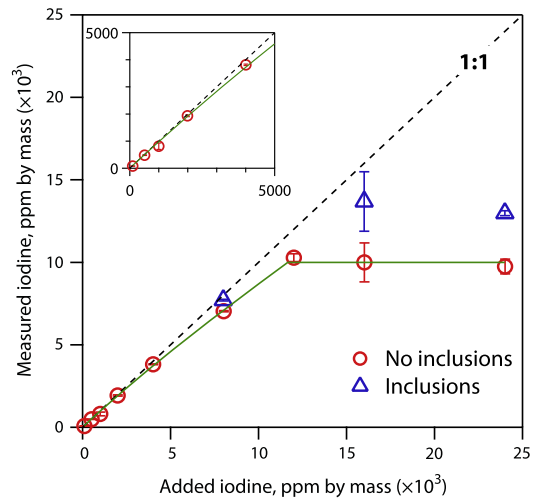


**Fig. 14.** Measured iodine concentration as a function of iodine loading. The green line represents the concentration dissolved in glass and the horizontal portion of green line represents iodine solubility. (For interpretation of the references to color in this figure legend, the reader is referred to the web version of this article.)

iodine solubility was determined to be ~10,000 ppm, by mass (1641 ppm iodine, by atom). As shown by XANES, the vast majority of iodine in the glass is present as iodide, and the solubility measurement is primarily for this species. Several other conclusions can be drawn from Fig. 14. First, the measured versus targeted iodine follows a linear (measured:target ratio = 1:1) trend from 99.4 to 1988 ppm iodine, but then deviates slightly up to 11,999 ppm ( $y = 0.808x$ ) resulting from the loss of iodine in the head space above the melt, separation of salt from the melt, and potential partitioning of iodine into bubbles. Secondly, the measurements performed on specimens with inclusions show higher, but not consistently higher, values with increased iodine loadings. Finally, when the amount of added iodide exceeded the thermodynamic solubility, a separate mixed salt phase containing  $\text{NaI}$ ,  $\text{Na}_2\text{SO}_4$ , and  $\text{KI}$  formed at the top of the melt.

### 3.6. Implications of this work

The issue of salt not being fully incorporated into glass melts has been studied for decades. In low or even moderate concentrations, mixtures of alkali sulfates and halides have a beneficial effect on the melting rate of glass, assisting with mass and heat transfer processes [14,38]. However, at excessively high concentrations, these salts can float on the top surface of the glass and plate out on the cold shoulders of the canisters or remain trapped in the glass as inclusions with general compositions of  $(\text{Na,K,Cs})(\text{Cl,I,F})$ ,  $(\text{Na,K,Cs})_2\text{SO}_4$ , and  $(\text{Na,K,Cs})\text{BO}_2$  [15,16]. Also, due to the low viscosity and high volatility of these salts, they often accumulate in the off-gas plenum [15,16,38,39]. Thus, it is important that the quantities of these salts are controlled during processing of the glass to keep the proper balance between maintaining an ideal melt rate and minimizing the accumulation of salt on the surface of the melt or as inclusions within the glass.

It is important to note the differences between the experiments discussed here and an actual melter scenario for nuclear waste glass processing that include processing temperature, atmospheric conditions, and volatility control. The processing temperature used for the experiments presented here was 1000 °C while the typical melter operating temperature is 1150 °C. The temperature selected for the current experiments was lower to limit the pressure inside of the sealed ampoule for safety concerns. The atmospheric conditions chosen for the experiments in the current work was an

evacuated quartz tube to eliminate the possibility of having iodine completely leave the vicinity around the melt. While the experiments in the current study were conducted under vacuum, the effect on redox of the melt due to this was likely negligible because of the long time required to reach true equilibrium. Thus, the true aim of this study was to determine the solubility of iodine in low-activity borosilicate glass at 1000 °C and, while the data was not collected at true equilibrium, the results show that the solubility will likely not be the limiting factor for iodine incorporation. In fact, the solubility of iodine was much higher than initially expected in this particular LAW glass composition.

#### 4. Conclusions

The solubility of iodine in a LAW borosilicate glass was determined in evacuated and sealed fused quartz ampoules heated at 1000 °C for 2 h. Under these conditions, loss of elemental iodine was minimized, and iodine was primarily present as iodide. Iodine loadings ranged 99.4–24,005 ppm, by mass. The solubility of iodine measured in the present study was determined to be 10,000 ppm iodine by mass (1641 ppm by atom), and is much higher than previously reported for a comparable glass (~2000 ppm iodine). Note that, although the previously reported iodine solubility was 2000 ppm, the measured values ranged up to 8500 ppm, which is much closer to the values we obtained. This difference likely results from the volatility of iodine during the previous experiments because they were run in open crucibles. Thus, the current experiments were designed to measure solubility whereas the previous experiments, while designed to measure solubility, instead likely measured retention, comparable to what would be experienced in a melter bubbled with air where both solubility and volatility play a role. Because the estimated iodine concentration in Hanford LAW glass is roughly 0.3 ppm, on average, if 100% is retained (based on the projected total mass of <sup>129</sup>I, 180 kg [17]), and the estimated total mass of low-activity waste glass to be produced,  $5.3 \times 10^8$  kg [40]), it can be concluded that the retention of iodine in LAW glass is not limited by solubility but by volatility.

However, based on the results from this study, we cannot conclude that iodine will be effectively retained during production of LAW glass. In the present study, some volatility was observed because elemental iodine was formed, presumably resulting from a redox couple with Fe<sub>2</sub>O<sub>3</sub> in the glass frit. During production of LAW glass, conditions in the glass are expected to be highly oxidizing because of the decomposition of nitrate and bubbling of air through the melt. These conditions may decrease the retention of iodine in the waste glass due to oxidation of iodide to elemental iodine, which is volatile under these conditions, as observed in this study.

#### Acknowledgements

This work was supported by the U.S. Department of Energy's (DOE) Waste Treatment and Immobilization Plant Project of the Office of River Protection. The authors thank Clyde Chamberlin and Shelley Carlson for helping prepare the specimens for analyses as well as David Pierce, Jesse Lang, and Steven Luksic for their optical microscopy documentation. Pacific Northwest National Laboratory (PNNL) is operated by Battelle Memorial Institute for the DOE under contract DE-AC05-76RL01830. A portion of the research was performed using capabilities in the William R. Wiley Environmental Molecular Sciences Laboratory, a national scientific user facility sponsored by DOE's Office of Biological and Environmental Research and located at PNNL. Portions of this work were performed at Lawrence Berkeley National Laboratory under Contract DE-AC02-05CH11231. Portions of this research were carried out

at the Stanford Synchrotron Radiation Lightsource, a Directorate of SLAC National Accelerator Laboratory and an Office of Science User Facility operated for DOE's Office of Science by Stanford University.

#### References

- [1] W.K. Kot, H. Gan, I.L. Pegg, in: G.T. Chandler, X.D. Feng (Eds.), *Proc. of the Env. Issues Waste Manag. Tech. Ceram. Nucl. Ind.: Ceram. Trans.*, vol. 107, 1999, pp. 441–449.
- [2] G.K. Sullivan, M.H. Langowski, P. Hrma, in: V. Jain, R.A. Palmer (Eds.), *Proc. of the Ceram. Trans: Env. Issues Waste Manag. Tech. Ceram. Nucl. Ind.*, vol. 61, Cincinnati, OH, 1996, pp. 187–193.
- [3] J.D. Vienna, P. Hrma, W. Buchmiller, J. Muller, *Preliminary Investigation of Sulfur Loading in Hanford LAW Glass. PNNL-14649, Pacific Northwest National Laboratory, Richland, WA, 2004.*
- [4] I.L. Pegg, H. Gan, I.S. Muller, D. McKeown, K. Matlack, Summary of Preliminary Results on Enhanced Sulfate Incorporation During Vitrification of LAW feeds. VSL-00R3630-1, Rev. 2, ORP-54333, Vitreous State Laboratory, The Catholic University of America, Washington, DC, 2008.
- [5] R. Goles, J. Perez, B. Maclsaac, D. Siemer, J. McCray, *Test Summary Report INEEL Sodium-Bearing Waste Vitrification Demonstration – RSM-01-1. PNNL-13522, Pacific Northwest National Laboratory, Richland, WA, 2001.*
- [6] H. Li, P. Hrma, J.D. Vienna, in: D.R. Spearing, G.L. Smith, R.L. Putnam (Eds.), *Proc. of the Env. Issues Waste Manag. Tech. Ceram. Nucl. Ind.*, vol. 119, St. Louis, MO, 2000, pp. 237–245.
- [7] P. Hrma, J. Vienna, J. Ricklefs, in: R.J. Finch, D.B. Bullen (Eds.), *Proc. of the Mat. Res. Soc. Symp. – Sci. Basis Nucl. Waste Manage*, vol. XXVI, 757, Boston, MA, 2002, pp. 147–158.
- [8] P. Hrma, J. Vienna, W. Buchmiller, J. Ricklefs, in: J.D. Vienna, D.R. Spearing (Eds.), *Proc. of the Env. Issues Waste Manag. Tech. Ceram. Nucl. Ind. IX – Ceram. Trans.*, vol. 155, Nashville, TN, 2003, pp. 93–100.
- [9] C.M. Jantzen, M.E. Smith, D.K. Peeler, in: J.D. Vienna, C.C. Herman, S. Marra (Eds.), *Proc. of the Environmental Issues and Waste Management Technologies in the Ceramic and Nuclear Industries X*, vol. 168, Indianapolis, IN, 2004, pp. 141–152.
- [10] D. Caurant, P. Loiseau, O. Majerus, V. Aubin-Chevaldonnet, I. Bardez, A. Quintas, *Glasses, Glass-Ceramics and Ceramics for Immobilization of Highly Radioactive Nuclear Wastes*, Nova Science Publishers, New York, 2009.
- [11] G. Calas, M. Le Grand, L. Galoisy, D. Ghaleb, *J. Nucl. Mater.* 322 (1) (2003) 15–20.
- [12] G.N. Greaves, *J. Non-Cryst. Solids* 71 (1–3) (1985) 203–217.
- [13] R.K. Mishra, K.V. Sudarsan, P. Sengupta, R.K. Vatsa, A.K. Tyagi, C.P. Kaushik, D. Das, K. Raj, *J. Am. Ceram. Soc.* 91 (12) (2008) 3903–3907.
- [14] D.F. Bickford, A. Applewhite-Ramsey, C.M. Jantzen, K.G. Brown, *J. Am. Ceram. Soc.* 73 (10) (1990) 2896–2902.
- [15] C.M. Jantzen, *Inorganic Analysis of Volatilized and Condensed Species Within Prototype Defense Waste Processing Facility (DWPF) Canistered Waste. WSRC-TR-92-260, Westinghouse Savannah River Company, Aiken, SC, 1992.*
- [16] C.M. Jantzen, *Glass Melter Off-Gas System Pluggages: Cause, Significance, and Remediation. WSRC-TR-90-205, Westinghouse Savannah River Company, Aiken, SC, 1991.*
- [17] F.M. Mann, *Annual Summary of the Integrated Disposal Facility Performance Assessment for 2004. DOE/ORP-2000-19, Rev. 4. CH2M Hill Hanford Group, Richland, WA, 2004.*
- [18] P.R. Hrma, *Retention of Halogens in Waste Glass. PNNL-19361. Pacific Northwest National Laboratory, Richland, WA, 2010.*
- [19] S.N. Crichton, M.F. Savage, M. Tomozawa, in: V. Jain, R. Palmer (Eds.), *Proc. of the Ceram. Trans: Env. Issues Waste Manag. Tech. Ceram. Nucl. Ind.*, vol. 61, The American Ceramics Society Inc., Westville, OH, 1995, pp. 291–298.
- [20] H. Abramowitz, M. Brandys, R. Cecil, N. D'Angelo, K.S. Matlack, I.S. Muller, I.L. Pegg, R.A. Callow, I. Joseph, *Technetium Retention in WTP LAW Glass with Recycle Flow-Sheet DM10 Melter Testing VSL-12R2640-1 Rev. 0. RPP-54130, Washington River Protection Solutions, Richland, WA, 2012.*
- [21] S.N. Crichton, T.J. Barbieri, M. Tomozawa, in: V. Jain, R. Palmer (Eds.), *Proc. of the Ceram. Trans: Env. Issues Waste Manag. Tech. Ceram. Nucl. Ind.*, vol. 61, The American Ceramics Society, Inc., Westville, OH, 1995, pp. 283–290.
- [22] B.J. Riley, B.T. Rieck, J.S. McCloy, J.V. Crum, S.K. Sundaram, J.D. Vienna, *J. Nucl. Mater.* 424 (1–3) (2012) 29–37.
- [23] W.M. Haynes, Y.-R. Luo (Eds.), *CRC Handbook of Chemistry and Physics, 91st ed.*, CRC Press/Taylor and Francis, Boca Raton, FL, 2011.
- [24] C.Z. Soderquist, M.J. Schweiger, D.-S. Kim, W.W. Lukens, J.S. McCloy, *J. Nucl. Mater.* (2014). doi: 10.1016/j.jnucmat.2014.03.008. (in press).
- [25] J.S. McCloy, B.J. Riley, A. Goel, M. Liezers, M.J. Schweiger, C.P. Rodriguez, P. Hrma, D.-S. Kim, W.W. Lukens, A.A. Kruger, *Environ. Sci. Technol.* 46 (22) (2012) 12616–12622.
- [26] K.S. Matlack, I. Joseph, W.L. Gong, I.S. Muller, I.L. Pegg, *Glass Formulation Development and DM10 Melter Testing With ORP LAW Glasses. VSL-09R1510-2, Vitreous State Laboratory, The Catholic University of America, Washington, D.C., 2009.*
- [27] K.S. Matlack, I.S. Muller, I.L. Pegg, I. Joseph, *Improved Technetium Retention in Hanford LAW glass – Phase 1. VSL-10R1920-1, Vitreous State Laboratory, The Catholic University of America, Washington, DC, 2010.*

- [28] C.F. Brown, K.N. Geiszler, T.S. Vickerman, *Anal. Chem.* 77 (21) (2005) 7062–7066.
- [29] S. Webb, <[http://ssrl.slac.stanford.edu/~swebb/spdocs/sixpack\\_documentation.htm](http://ssrl.slac.stanford.edu/~swebb/spdocs/sixpack_documentation.htm)>, 2010.
- [30] B. Ravel, M. Newville, *Phys. Scripta T115* (2005) 1007–1010.
- [31] B.J. Riley, J.S. McCloy, A. Goel, M. Liezers, M.J. Schweiger, J. Liu, C.P. Rodriguez, D.-S. Kim, *J. Am. Ceram. Soc.* 96 (4) (2013) 1150–1157.
- [32] Y.S. Shimamoto, Y. Takahashi, *Anal. Sci.* 24 (3) (2008) 405–409.
- [33] W.A. Reed, I. May, F.R. Livens, J.M. Charnock, A.P. Jeapes, M. Gresley, R.M. Mitchell, P. Knight, *J. Anal. At. Spectrom.* 17 (5) (2002) 541–543.
- [34] M. Fuhrmann, S.A. Bajt, M.A.A. Schoonen, *Appl. Geochem.* 13 (2) (1998) 127–141.
- [35] D. Kim, M.J. Schweiger, *J. Non-Cryst. Solids* 379 (2013) 123–126.
- [36] M.T. Weller, G. Wong, *Eur. J. Solid State Inorg. Chem.* 26 (1989) 619–633.
- [37] R.W. Cheary, A.A. Coelho, J.P. Cline, *J. Res. Natl. Inst. Stand. Technol.* 109 (1) (2004) 1–25.
- [38] H.L. Hull, *Slurry-Fed Melter Tests, Memorandum, DPST-84-518, Savannah River Laboratory, Aiken, SC, 1984.*
- [39] H.L. Hull, *Slurry-Fed Melter Test, Memorandum, DPST-82-532, Savannah River Laboratory, Aiken, SC, 1982.*
- [40] P.J. Certa, P.A. Empey, *River Protection Project System Plan. ORP-11242, Rev. 6. Office of River Protection, US Department of Energy, Richland, WA, 2011.*